# Loss of Fnip1 Results in Renal Cyst Formation and Synergizes with TSC1 Loss to Promote mTORC1 Activation

Ryan M. Centini

A thesis
submitted in partial fulfillment of the
requirements for the degree of

Master of Science

University of Washington
2017

Committee:
Brian M. Iritani
H. Denny Liggitt
Alanna Ruddell

Program Authorized to Offer Degree:
The Department of Comparative Medicine

University of Washington

**Abstract**

Loss of Fnip1 Results in Renal Cyst Formation and Synergizes with TSC1 Loss to Promote mTORC1 Activation

Ryan M. Centini

Chair of the Supervisory Committee:
Brian M. Iritani
Department of Comparative Medicine

Birt-Hogg-Dube' Syndrome (BHDS) is a rare genetic disorder in humans characterized by increased risk for renal tumors. BHDS is caused by mutations in the *BHD* gene, which encodes for Folliculin, and cytoplasmic adapter protein which binds to two other proteins called FNIP1 and FNIP2 (Folliculin interacting proteins-1 and -2) as well as AMP kinase (AMPK). AMPK is an important energy sensor for the cell, and once activated stimulates energy production while inhibiting mTOR. Whereas kidney-specific deletion of the *Bhd* gene in mice is known to result in polycystic kidney disease and renal cell carcinoma, the roles of Fnip1 in renal cell development and function are unclear. In this study, we utilized mice with constitutive deletion of the *Fnip1* gene to show that the loss of Fnip1 alone is sufficient to cause a polycystic kidney disease, which was characterized by increased mTOR activation and metabolic hyperactivation. In addition, we found that loss of Fnip1 alone resulted in many cellular and molecular changes previously suggested as contributing to the development of PKD in humans, including alterations in ion channels and amino acid transporters, increased cell adhesion, and increased inflammation. Our results collectively define a novel role of Fnip1 in regulating kidney development and function, and provide a model for how Fnip1 regulates renal cell function.

# Table of Contents

## List of Figures

## Acronyms and Abbreviations

4EBP1- Eukaryotic Translation Initiation Factor 4E-Binding Protein 1
ACC-Acetyl CoA Carboxylase
ADPKD- Autosomal dominant polycystic kidney disease
AKT- Protein Kinase B
AMPK- AMP activated protein kinase
ATP- Adenosine Triphosphate
ATP5g1- ATP Synthase
BHDS- Birt-Hogg-Dube' Syndrome
cAMP- cyclic Adenosine Monophosphate
CFTR- Cystic Fibrosis Transmembrane Receptor
DHAP- Dihydroxyacetone phosphate
ECAR- Extracellular Acidification Rate
ENU-N-ethyl-N-nitrosourea
Erk- Extracellular Signal-Regulated Kinase
FCLN- Folliculin
Fnip1- Folliculin Interacting Protein 1
Fnip2- Folliculin Interacting Protein 2
GAPDH-Glyceraldehyde 3-Phosphate Dehydrogenase
GSK3-Glycogen Synthase Kinase 3
KEGG- Kyoto Encyclopedia of Genes and Genome
LBK1- Liver Kinase B1 (AKA Serine/threonine kinase 11)
LC-MS- Liquid Chromatography Mass Spectrometry
MMP- Matrix Metaloproteinases
mTOR- Mammalian target of rapamycin
mRNA- Messenger RNA
NKCC1- $Na^{+}$-$K^{+}$-$2Cl^{-}$ Cotransporter
OCR- Oxygen Consumption Rate
OXPHOS- Oxidative phosphorylation
PC1- Polycystin 1
PC2- Polycystin 2
PGC1a-Peroxisome Proliferator-Activated Receptor Gamma Coactivator 1-Alpha
PPARg- Peroxisome Proliferator-Activated Receptor Gamma
Raf- Rapidly Accelerated Fibrosarcoma
RNAseq- RNA sequencing
Raptor- Regulatory-Associated Protein of mTOR
Rheb- Ras Homolog Enriched in Brain
ROS- Reactive Oxygen Species
RT-PCR – Real Time Polymerase Chain Reaction
S6R- S6 Ribosomal Protein
SEM- Standard Error of the Mean
Slc- Solute Carrier
STAT3- Signal Transducer and Activator of Transcription 3
TCA- Tricarboxylic Acid cycle
TLR- Toll-like Receptor

TSC1- Tuberous Sclerosis 1
TSC2- Tuberous Sclerosis 2

**Acknowledgements**

This study was supported by NIH grants R56 AI092093, R21 AI109020, R01 AI092093, and by generous support from the Department Chairman Denny Liggitt. I thank Brian Johnson from the Histology and Imaging Core for assistance with immunohistochemistry.

Thanks also to Dr. David Hockenbery and Dr. Daciana Margineantu for their help with the Seahorse assay as well as Dr. Daniel Raftery and Dr. Haiwei Gu for their assistance with mass spectrometry measurements.

Finally thanks to the wonderful research team in the Iritani lab:
Dr. Terri Iwata, Dr. Julita Ramirez, Dr Heon Park, Mark Tsang, and Brandon Iritani

As well as to my mentor Dr. Brian Iritani, without whom none of this research would have been possible.

## Dedication

This is dedicated to my wife for her support during the years I have dedicated to developing my career, and to my parents for inspiring, encouraging, and supporting my love and interest in science and animals.

## Introduction

Birt-Hogg-Dube' Syndrome (BHDS) is a rare autosomal dominant disorder in which affected individuals are at high risk of developing cutaneous fibrofolliculomas and bilateral pulmonary cysts, which can rupture resulting in severe pneumothoraces(Goncharova et al., 2014). BHD patients are also at high risk for developing renal tumors of a variety of histological types including most commonly chromophobe renal cell carcinoma, but also clear cell renal carcinoma, oncocytoma, and papillary renal cell carcinoma (Pavlovich et al., 2002). In 2002, BHDS was localized to germline mutations in the *BHD* gene encoding a novel tumor suppressor Folliculin (FLCN) (Nickerson et al., 2002). Additional molecular studies revealed that the FLCN protein binds to two structurally related proteins called FNIP1 and FNIP2 (Folliculin interacting proteins-1 and -2), as well as the master metabolic regulator AMP kinase (AMPK). In particular, FNIP1 and FNIP2 bind to the C terminus of FLCN and also to AMP-activated protein kinase (AMPK). AMPK is an important energy sensor that is activated in response to low energy (ATP/high AMP), via phosphorylation at threonine 172 by LKB1 kinase, and also by allosteric activation by AMP. One activated, AMPK stimulates energy production in part by stimulating mitochondrial biogenesis, fatty acid oxidation, glucose uptake, and autophagy, while also inhibiting energy consumption by negatively regulating mechanistic target of rapamycin (mTOR). Specifically, AMPK phosphorylates and inhibits the essential mTOR co-activator Raptor, and phosphorylates and stimulates TSC1, a negative regulator of mTOR. While the exact roles of Folliculin in modulating these pathways are not clear, Folliculin has been implicated in both inhibition and activation of AMPK, inhibition of mitochondrial biogenesis, inhibition and activation of autophagy, and inhibition and activation of mTOR.

Because constitutive deletion of *Flcn* in mice results in early embryonic death (Hasumi et al., 2009), the majority of studies in murine models involve either analyses of *Flcn* heterozygous mice, or by conditionally deleting *Flcn* in a tissue specific manner using the Cre-LoxP system. Hasumi et al found the heterozygous *Flcn* mice developed PKD, which progressed to renal cancer with a median tumor-free survival of 25 months. Similar to BHDS, histological types of tumors from $Flcn^{+/-}$ mice include oncocytic hybrid, oncocytoma, and clear cell tumors, which were defined by, increased activation of mTOR. Two studies using a conditional kidney knockout of *Flcn* in the distal tubules of mice found that mice developed polycystic kidney disease, which progressed to renal failure by 3 weeks of age. Both studies showed that there was pronounced upregulation of the AKT/mTOR signaling pathways following disruption of *Bhd*, and that treatment with the mTORC1 inhibitor rapamycin could rescue the phenotype (Chen et al., 2008; Hasumi et al., 2008). However, in the second study, they found that the PKD phenotype could progress to renal cell carcinomas (Chen et al., 2008). A more recent model involving the use of a conditional knockout of FLCN in the proximal tubules showed a less severe polycystic phenotype beginning at 6 months of age, which progressed to the development of a variety renal tumors including; papillary, sarcomatoid, chromophobe, and clear cell renal cell carcinomas. These mice also developed oncocytomas and hybrid oncocytoma/chromophobe tumors (Chen et al., 2015). Lastly a study utilizing conditional kidney *Flcn* knockout from the distal tubules found the development of PKD, which correlated with increased mitochondrial metabolism. Disruption of the *Ppargc1* partially rescued the PDK phenocyte in *Flcn* deficient mice (Hasumi et al., 2012). Collectively, these studies suggest that disruption of Folliculin is sufficient to result in the development of PKD, which in some cases can progress to renal cancer, which is in part due to increased activation of the mTOR pathway.

Although the roles and importance of Folliculin in kidney development and function have been extensively investigated, the roles of Fnip1 and Fnip2 in kidney development and function are not as clear. Recently, one laboratory generated *Fnip1*, *Fnip2* double null mice, using a kidney specific strategy (Hasumi et al., 2015). They found no changes in the kidney development or function when either *Fnip1* or *Fnip2* were deleted alone, but when both were deleted together, the mice developed polycystic kidney disease that was fatal by 3 weeks of age. Interestingly, kidney specific deletion of *Flcn* did not augment kidney size or cystic histology of *Fnip1/Fnip2* double null kidneys, suggesting that Fnip and Flcn likely act on convergent pathways. The authors also showed heterozygous *Fnip1/*homozygous *Fnip2* null mice developed renal cancer at 24 months of age, which consisted of hybrid oncocytic tumors, similar to tumor types found in BHDS patients.

In this study, we investigated the specific roles of Fnip1 in renal development and function, using *Fnip1* null mice we previously generated using a random ENU mutagenesis strategy(Appleby and Ramsdell, 2003) in mice in mice to identify novel immune regulatory genes (Park et al., 2012). *Fnip1*$^{-/-}$ mice were identified by an absence of circulating B-lymphocytes, which was attributed to a block in B cell development and survival at the pre-B cell stage. Here, we found that loss of *Fnip1* results in slightly enlarged kidney size and significant increases in microcyst formation, which was defined by local increases in mTORC1 activation and increased glycolytic and oxidative metabolism of renal epithelial cells. The local cyst environment was defined by classical cellular and molecular changes attributed to the development of PKD, including increased immune cell infiltration, altered expression of ion channels and cell adhesion. Importantly, co-deletion of the mTORC1 inhibitor TSC1 resulted in greatly accelerated PKD development due to greatly increased activation of the mTOR pathway.

## Results

### Disruption of Fnip1 results in increased kidney weight and numbers of kidney cysts

Because inactivating mutations in the *BHD* gene encoding Folliculin result in renal cancer, we sought to determine if loss of Fnip1 alters kidney development and/or function. We found that kidney-to-brain weight ratios were significantly greater in *Fnip1*$^{-/-}$ mice (mean 0.53) (Fig. 1A) and *Fnip2*$^{-/-}$ mice (Fig. 1B) compared to wildtype mice (mean 0.32), indicating that loss of Fnip1 or Fnip2 resulted in increased kidney weight (Fig. 1A). Analyses of hematoxylin and eosin (H & E) stained histologic sections of kidney revealed that there were increased numbers of microcysts in the renal cortex of *Fnip1*$^{-/-}$ mice compared to WT mice (Figs. 1C and 1D). The microcysts were lined by renal tubular epithelium, which tended to form blebs into the cyst lumen. Loss of Fnip1 did not change urine specific gravity relative to WT mice, suggesting that renal function was not perturbed following disruption of Fnip1 (Supplemental Figure 1). These results collectively suggest that loss of Fnip1 alters renal development, leading to limited formation of renal cysts.

### Fnip1 loss results in focal increases in mTORC1 activity

Disruption of the *BHD* gene in mice results in polycystic kidney disease (PKD), characterized by increased mTORC1 activation. To determine why loss of Fnip1 could result in increased renal weight and cyst formation, we measured activation of AMPK and the mTOR pathways by immunoblotting and immunohistochemistry (IHC). Immunoblotting of whole kidney lysate from *Fnip1*$^{-/-}$ and WT mice did not reveal any significant changes in pAMPK, an indicator of

activated AMPK, or pS6R, a downstream target of mTORC1 activation (Fig. 2A). However, using IHC, we found local increases in P-S6R in the renal tubular epithelial cells lining the microcysts in the *Fnip1*$^{-/-}$ kidneys (Fig. 2B). mRNA expression of Fnip2 and Folliculin were unchanged (Fig. 2C), whereas expression of *PGC1α,* a master regulator of mitochondrial biogenesis, as well as a downstream target *Pparg* (Fig. 2D), were increased in *Fnip1*$^{-/-}$ versus WT kidneys. These results suggest that loss of Fnip1 results in increased mTORC1 activation and *Pgc1a* expression in renal epithelial cells, which may contribute to the development of PKD.

**Fnip1 deficient renal epithelial cells exhibit increased glycolysis and oxidative phosphorylation**

We next assessed whether loss of Fnip1 and subsequent mTORC1 activation altered the metabolic characteristics of *Fnip1* null renal epithelial cells. Renal tubular epithelial cells were isolated from *Fnip1*$^{-/-}$ and WT mice, and basal metabolic characteristics were measured using the Seahorse XF analyzer, which measures oxygen consumption rate (OCR; a measure of oxidative phosphorylation) and extracellular acidification rate (ECAR; a measure of glycolysis). *Fnip1*$^{-/-}$ renal tubular epithelial cells exhibited increased maximal ECAR (Fig. 3A) and OCR (Fig. 3B) relative to WT renal tubular epithelial cells, indicating that loss of Fnip1 results in increased basal metabolism.

In order to better define this observed metabolic shift, we took an unbiased global metabolomic approach using liquid chromatography tandem mass spectrometry (LC-MS/MS) to measure alterations in levels of metabolites associated with major metabolic pathways. We found that *Fnip1*$^{-/-}$ kidneys contained increased levels of metabolites derived from the amino acid

leucine (D-Leucic acid, 2-hydroxyisovaleric acid, and OH-Phenylpyruvate), a major inducer of mTORC1 activation, relative to WT kidneys (Fig. 3C). *Fnip1*$^{-/-}$ kidneys also presented with increased levels of glycolysis and TCA cycle metabolites including Aspartic Acid, DHAP and Oxaloacetate respectively. Increases were also seen in the purine metabolites 1-Methyladenosine, Xanthosine, and Allantoin (Fig. 3D), consistent with increased purine biosynthesis in *Fnip1*$^{-/-}$ kidneys. These results support increased metabolic activity following disruption of *Fnip1*(Fig. 2C), and also supports increased mTORC1 activation, which is a major driver of glycolysis and mitochondrial biogenesis.

**Global gene expression analyses reveals alterations in ion transport and immune cell infiltration**

To assess global mRNA changes associated with disruption of *Fnip1* in renal tissue, we performed RNAseq on kidney tissue from *Fnip1*$^{-/-}$ and WT mice, followed by quantitative PCR to confirm changes in gene expression of selected genes of interest. We found that mRNA expression of 651 genes were significantly different in *Fnip1*$^{-/-}$ kidney tissue versus *Fnip1*$^{+/-}$ tissue. Of the 651 genes, expression of 445 genes were upregulated and 206 genes were downregulated following disruption of Fnip1. Kyoto Encyclopedia of Genes and Genome (KEGG) analyses indicated that of the downregulated genes, there was significant enrichment for genes associated with sodium dependent ion transport, organic ion transport, and anion transmembrane transport (Fig. 4A). In contrast, of the upregulated genes, there was significant enrichment in expression of genes associated with cell adhesion and immune response (Fig. 4B). Quantitative PCR analyses confirmed that expression of many of the *Slc* family of transporter genes are being down regulated following disruption of Fnip1 (Fig 5A). For example,

expression of *Slc1a4* and *Slc17a3*, which are involved with glutamate transport, were both significantly decreased in *Fnip1*$^{-/-}$ versus *Fnip1*$^{+/-}$ tissue. Similarly, expression of *Slc13a5*, and *Slc24a3*, two genes involved with $Na^+$ transport, were also decreased in *Fnip1*$^{-/-}$ versus *Fnip1*$^{+/-}$ tissue. Four genes important for the transport of organic molecules in the proximal renal tubule were also decreased including *Slc22a2*, which resorbs organic cations; *Slc22a6* and *Slc22*a7, which are involved with the transport of anions; and *Slc22a12*, which transports urate for excretion and is important for proper kidney function. Of the *Slc* genes with increased expression, *Slc15a3* is a proton/oligopeptide cotransporter, and *Slc22a3* is an organic cation transporter that is expressed in several tissues including liver, intestine, nervous, and kidney. These results collectively suggest that loss of Fnip1 in renal tissue results in significant alterations in the expression of genes encoding ion transporters.

Our Seahorse and metabolomics analyses suggested that mitochondrial metabolism is increased in Fnip1 null tissue. Consistent with this notion, RNAseq and quantitative PCR data showed changes in multiple Acyl-CoA genes (Fig 5B). Acox3, Acsm 3, and Acss3 are all involved with fatty acid synthesis and were decreased in *Fnip1*$^{-/-}$ mice, whereas some genes associated with fatty acid metabolism were increased, including Acsf2, and Acsl6. Acss1 (acetyl-CoA synthetase) is important in the TCA cycle and was increased, while Acot12 which hydrolysis Acss1 was decreased. These increases in metabolic metabolites and the changes seen Acyl-CoA genes are consistent with increased mTORC1 signaling.

Recent studies suggest that increased kidney inflammation is associated with PKD in humans. Quantitative PCR confirmed that genes involved in immunity and inflammation were increased in *Fnip1*$^{-/-}$ renal tissue, including the S100 genes, Toll-like receptor (TLR) genes, and genes encoding complement (Fig 5C-E). Specifically, *Fnip1*$^{-/-}$ renal tissue was characterized by

increased expression of complement components including component 3 (*C3* and *C3ar1*), which are important in both the classical and alternate pathways of complement signaling, and *C1qa*, *b*, and *c*, which are all part of the *C1q* complex that is important in the classical pathway (Fig. 5C). Similarly, increases were seen in the expression of the *S100A14*, *S100A6*, *S100A8*, and *S100A9* pro-inflammatory genes (Fig. 5D). S100A14 affects the p53 pathway and modulates expression of matrix metaloproteinases MMP1 and MMP9. S100A6 in important in cell proliferation, cytoskeletal dynamics, and tumorigenesis, thus promoting cell division and tumor growth when overly expressed. S100A8 is highly expressed in the cytosol of some immune cells including neutrophils, macrophages, and dendritic cells, and is induced by toll-like receptor (TLR) agonists, and S100A9 inhibits myeloid differentiation thereby contributing to tumor growth. We also found that expression of *Tlr1*, *Tlr7,* and *Tlr13* were also increased in *Fnip1*$^{-/-}$ versus WT kidney tissue (Fig. 5E). Toll-like receptors are important for activation of the innate immune system by recognizing pathogen-associated molecular patterns in microbes.

To further determine whether disruption of Fnip1 was associated with increased inflammation in *Fnip1* null renal tissue, we purified immune cells from *Fnip1*$^{-/-}$ and WT kidney tissue and defined the representation of cells by flow cytometry (Fig. 6A). Compared to WT renal tissue, *Fnip1*$^{-/-}$ renal tissue showed a proportional increase in the representation of CD11c$^{+}$ and GR1$^{+}$ myeloid cells Fig (Fig 6A), whereas CD3$^{+}$ T cells were significantly different. The CD11c protein is expressed by myeloid cells (including macrophages), and GR1 protein is predominantly expressed by bone marrow and peripheral blood neutrophils. Interestingly, using IHC we found focal increases in F4/80 staining localized around the cysts of sections of kidney from *Fnip1*$^{-/-}$ relative to WT mice (Fig 6B). The F4/80 antigen is a glycoprotein that is expressed by murine macrophages. In contrast to our data on total T cells, we found focal

increases in CD3ε positive T cells around renal cysts. These results confirm that disruption of Fnip1 results in increased representation of inflammatory cells infiltrating Fnip1 deficient kidney tissue.

**Fnip1 and TSC1 synergize to inhibit mTORC1 activation and polycystic kidney disease**

Kidney tissue from human patients with BHDS, and murine kidney tissue from mice with gene-targeted mutations in *Bhd*, are characterized by increased mTORC1 activation. In murine models, increased mTORC1 expression is associated with the development of PKD, which responds to rapamycin treatment (Chen et al., 2008; Hasumi et al., 2008). These results suggest that disruption of Fnip1 might increase PKD development in part by increasing mTORC1 activation. However, recent studies whereby *Bhd*, *Fnip1*, or *Fnip2* were knocked down in cell lines suggested that the Folliculin/Fnip1/Fnip2 complex may be required to activate mTORC1, in part by recruiting the complex to the lysosome where it is activated by Rheb-GTP and the TSC pathway. To further assess how disruption of Fnip1 modifies mTORC1 signaling and PKD in vivo, we generated a murine model of PKD, whereby the mTORC1 inhibitor *TSC1* gene was disrupted using *Mb1*Cre, which is predominantly expressed in hematopoietic cells and to a lesser extent in kidney. We then bred $Fnip1^{-/-}$ mice to $TSC1^{fl/fl}Mb1$Cre mice and defined the consequences of *Fnip1* loss on mTOR signaling and the development of PKD. $Tsc1^{fl/fl}Mb1Cre$ alone developed significant PKD by 10 weeks of age (Fig. 7A and B) characterized by a ~ 2-fold increase in kidney/brain weight ratio (Fig. 7C) and increased cystic structures, which progresses to a ~5-fold increase in kidney/brain weight by 10 weeks of age (Fig. 7C). Analyses of renal tissue from 12 week-old $Tsc1^{fl/fl}Mb1Cre$ and age matched wildtype mice revealed significantly increased Erk-phosphorylation and decreased AKT-308 phosphorylation, consistent with the

known ability of activated mTOR signaling to autoregulate itself through inhibition of PI3 kinase signaling (Fig. 7E). Phosphorylation of S6R and 4EBP1, downstream targets of mTORC1 signaling, were also significantly increased in *Tsc1*$^{fl/fl}$*Mb1Cre* mice relative to age matched wildtype mice. To define how loss of Fnip1 modulates activated mTOR signaling in *Tsc1* null mice, we determined how *Fnip1* deficiency altered kidney-to-brain weight ratios in *Tsc1* null mice (*Fnip1*$^{-/-}$ *Tsc1*$^{fl/fl}$*Mb1Cre)* mice compared to *Tsc1*$^{fl/fl}$ *Mb1-Cre*$^{+}$ mice alone. *Tsc1Fnip1* double null mice developed large cystic kidneys (kidney/brain ratio mean 1.79) by 4 weeks of age (Figs. 8A and B) whereas *Tsc1* null mice had normal appearing kidneys at 4 weeks (Figs. 7C), and did not develop cystic kidneys of comparable size as *Tsc1Fnip1* double null mice until 10 weeks of age. While the *Tsc1* null mice survived an average of 24 weeks until euthanasia (Fig. 7D), *Tsc1Fnip1* double null mice only survived to 4-6 weeks of age before euthanasia was required (Fig. 8C). Immunoblot analysis revealed increased phosphorylated ribosomal S6 protein (S6R) (~ 2-fold) in *Tsc1Fnip1* double null mice relative to *Tsc1*$^{-/-}$ mice, and significantly higher levels relative to *Fnip1*$^{-/-}$, and WT mice (Fig. 8D). Interestingly, phosphorylated EIF4E-binding protein 1 (P-4EBP1) levels were approximately 10-fold higher than either *Tsc1*$^{-/-}$ kidneys or *Fnip1*$^{-/-}$ kidneys. These results indicate that there is strong synergism between loss of Fnip1 and loss of TSC1, and suggest that these pathways utilize to activate mTORC1 may be divergent.

**Discussion**

In Birt Hogg Dube' syndrome, genetic alterations in the *BHD* gene encoding Folliculin result in diverse array of disease syndromes including lung and kidney cysts, pneumothorax, fibrofolliculomas, and renal cancers. Here we present evidence that loss of Folliculin interacting protein 1 alone is sufficient to initiate early polycystic kidney disease, as well as many of the cellular and molecular changes that have been associated with the development of PKD in humans. These results provide support that Folliculin and Fnip1 function on similar molecular pathways, but that Folliculin, Fnip1, and Fnip2 cannot completely compensate for the absence of each other. We also provide support for the cellular and molecular mechanisms whereby Folliculin, Fnip1, and Fnip2 may regulate kidney functions, and how their loss may contribute to the development of PKD and renal cancers in humans.

Autosomal dominant polycystic kidney disease (ADPKD) is genetic disease characterized by kidney cysts and eventually renal failure. ADPKD is caused by mutations in either the *Pkd1* or *Pkd2* genes, which encode Polycystin 1 (PC1) and Polycystin 2 (PC2) respectively. PC1 is a 450 kD protein with a large extracellular domain, 11 membrane spanning domains, and a short c-terminus. The large extracellular domain membrane and subcellular location and junctional complexes, suggests PC1 is important for cell-cell and cell-matrix interactions. The *Pkd2* gene product Polycystin 2 (PC2), a 968 aa protein that has 6 transmembrane domains, and functions as a calcium permeable non-selective cation calcium channel which is homologous to the transient receptor potential family of cation channels. The majority of the PC2 protein resides intracellularly where it regulates cytoplasmic calcium levels through interactions with the ryanodine and $IP_3$ receptors. The PC1 and PC2 complex localize to

primary cilium, where the complex is believe to be activated on cilia by waves of flow, which transmits signals intracellularly to release calcium from intracellular stores. Mutations in *Pkd*1 or *Pkd2* alters intracellular signaling and cell matrix interactions, resulting in kidney epithelial cells reorganizing themselves into spherical rather than tubular structures, which then fill with fluid and expand the developing cysts. One model for how tubular epithelial cells reorganize from tubular to spherical morphology posits that loss of cell polarity (through changes in cell adhesion) causes epithelial cells to stop dividing along the axis parallel to the tubule lumen, and divide excessively in a circular pattern. Increased cell division, which is a major feature of ADPKD, and driven in part by increased activation of mTOR, a major driver of cellular growth required to support cell division. Studies have shown a link between PC1 and mTOR, whereby the cytoplasmic tail of PC1 interacts with Tuberin, the protein product of the *TSC2* gene. Although the details have not been worked out, it has been proposed that PC1 sequesters the mTORC1complex together with Tuberin, which in turn inhibits mTOR (Pema et al., 2016; Shillingford et al., 2006). Mutations in PC1 release Tuberin from mTOR, allowing mTORC1 to become activated (Mostov, 2006). Another mechanism for mTORC1 activation in ADPKD, is due to co-deletion of the *TSC2* gene along with *PKD1*, since both are located adjacent to each other on the chromosome (Seeger-Nukpezah et al., 2015). Biochemical analyses of kidney tissue from various murine models of PKD have shown that there is significant hyperactivation of mTOR, and that inhibiting mTOR with Rapamycin can reduce the severity of PKD (Hartman et al., 2009; Shillingford et al., 2006). Conversely, kidney specific disruption of the *TSC1* or *TSC2* genes in mice results in increased mTORC1 activation and severe PKD, which can be completly rescued by treatment with Rapamycin (Zhou et al., 2009).

Another major driver of increased epithelial cell division in ADPKD is the proto-oncogene c-Myc, which is increased in mouse models of PKD (Harris and Torres, 2014). One study showed that transgenic expression of c-Myc is sufficient to cause cyst formation in the kidneys (Trudel et al., 1991). Both c-Myc and mTOR are major drivers of the Warburg Effect, whereby mostly cancer cells switch their metabolic preferences from mostly oxidative phosphorylation, which produces mostly ATP, to aerobic glycolysis, which generates precursors such as amino acids, nucleic acids, and lipids required to fuel cell division. Increased aerobic glycolysis has been also linked to ADPKD, driven in part by increased c-Myc and mTORC1 activation, and through loss of LKB1, which is required for AMPK activation (Han et al., 2016). Kidney specific deletion of *LKB1*, which prevents AMPK activation and results in excessive mTOR activation, also results in cyst development in the kidneys. Treatment of mice with non-metabolizable 2-deoxyglucose (2-DG), which inhibits glycolysis, also limits cyst formation.

Other signaling pathways activated by the PC1/PC2 complex and are believed to modulate ADPKD, include activation of the Janus kinases (JAK) and STAT/STAT3 transcription factors, which stimulate p21 expression to inhibit cell division; inhibition of Ras/Raf/Erk signaling, which modifies proliferative and apoptotic stimuli; and non-canonical Wnt signaling, which promotes cell polarity, for review see (Chapin and Caplan, 2010). Loss of each of these signaling pathways has been implicated in the pathogenesis of ADPKD.

Following reorganization of epithelial cells into spherical cysts due in part to excessive cell proliferation, conversion from an ion absorptive to an ion secretory epithelium causes ion secretion into the cyst lumen, which causes the cysts to fill with fluid. In normal renal epithelial cells, the apical cAMP activated cystic fibrosis transmenbrane receptor (CFTR) transport chloride ions into the lumen, which stimulates potassium transport back into the epithelial cell by

the $Na^+$-$K^+$-$2Cl^-$ (NKCC1) co-transporter. The lumen-negative potential generated by the chloride and potassium conductance drives sodium passively back into the lumen through a paracellular pathway. The net increase in sodium and chloride in the lumen leads to fluid accumulation by osmotic forces. In ADPKD, the ion secretory epithelium is defined by many changes in expression of the CFTR, as well as the NKCCl transporter encoded by *slc12a1*, and -*a2*, changes are also seen in $Ca^{2+}$ cation channels. AMPK negatively regulates the CFTR and Cl- secretion. Activation of AMPK with metformin inhibits CFTR secretion and reduces cyst growth. Although the roles of other ion transporters in ADPKD have not been addressed, theoretically alterations of any ion concentrations in the lumen would likely alter cyst development.

More recently, the roles of inflammatory cells in the development of ADPKD have been investigated with interesting results. In particular, activation of STAT3 and NFkB pathways in kidney epithelial cells (discussed above) stimulate the production and release of chemokines such as MCP1 and osteopontin, which attract monocytes and activate resident macrophages to a pro-inflammatory phenotype, which further activates TH1 T lymphocytes to release inflammatory mediators such as IFN-γ. Kidney macrophages, which are uniquely situated in close opposition to endothelial cells and basement membrane, switch from M1 macrophages to alternatively activated M2 macrophages, which produce TGf-β, and connective tissue growth factor (CTGF) that promote tubular epithelial cell proliferation and fibrogenesis. M1 macrophages also contribute to epithelial cell damage by producing ROS, TNF-α, IL-1, IL-6, and MMPs. Importantly, depletion of macrophages was shown to inhibit epithelial cell proliferation and cyst growth and improve renal function (Anders and Ryu, 2011; Karihaloo et al., 2011). These results suggest that immune cell infiltration can play a unique and important

role in the pathogenesis of PKD, by producing proflammatory mediators in response to tissue damage.

Folliculin interacting protein 1 was discovered based on physical interaction with Folliculin, Fnip2, and AMPK. Although tissue specific disruption of Folliculin is known to result in severe PKD and eventually renal cancer in mice, a role for Fnip1 has not been previously demonstrated. Remarkably, we found that disruption of *Fnip1* alone is sufficient to initiate many of the features implicated in PKD in humans. In addition, these changes manifest prior to the development of significantly large renal cysts. Firstly, using RNAseq, we found amongst 446 genes with increased expression, that the most significantly increased class of genes were involved in cell-cell adhesion, a major feature of PC1 signaling. Increased cell adhesion or cell-matrix adhesion could result in altered polarity and loss of axis of normal proliferation. Secondly, we found that loss of Fnip1 was sufficient to drive many of the signaling pathways, which enhance epithelial cell proliferation. Fnip1 loss resulted in increased mTOR specifically in epithelial cells surrounding renal cysts. This correlated with altered cellular metabolism as defined by increased oxidative phosphorylation and glycolysis in cultured primary epithelial cells in *Fnip1*$^{-/-}$ mice relative to WT mice. Metabolomics further reveal enrichment for metabolites associated with glycolysis and mitochondrial function. RNAseq analyses revealed that the most significant enrichments in transcription factor binding amongst the genes that changed in expression involved enrichment of c-Myc binding sites amongst upregulated genes. These results suggest that loss of Fnip1 alone is sufficient to stimulate the two major drivers of cellular growth, proliferation, and the Warburg effect: mTORC1 and c-Myc. Thirdly, loss of Fnip1 significantly alters the expression of numerous genes encoding ion and other transporters. Our RNAseq and quantitative PCR data indicates that 206 genes were downregulated following

disruption of Fnip1, there was highest enrichment for genes associated with sodium dependent ion transport, organic ion transport, and anion transmembrane transport. These results suggest that one of the major functions of Fnip1 is to control ion transport, which could play a major role of PKD development following disruption of Fnip1. Finally, our RNAseq, quantitative PCR, IHC, and flow cytometric results suggest that disruption of Fnip1 results in significant kidney inflammation, specifically in the regions surround cysts. By IHC, we see significant enrichment of F4/80 positive macrophages immediately surrounding cysts, and CD3+ T cells also appear to localize in similar regions. Using RNAseq and quantitative PCR, we found significant enrichment for genes involved in immune responses, including genes encoding complement components, Toll-like receptors, and S100 proinflammatory proteins. By flow cytometry, we found significant enrichment for myeloid cells in *Fnip1*$^{-/-}$ versus wildtype kidneys. These results suggest that Fnip1 normally may potently suppresses many cellular and molecular pathways associated with the development of PKD.

We also found that Fnip1 potently modulates mTORC1 activation, which addresses a major controversy as to whether Fnip1 is important for activating or inhibiting mTOR. Using siRNA knockdown approaches in human cell lines, three groups have presented evidence that Folliculin/Fnip regulates the recruitment of mTOR to the lysosome, where it is activated in response to amino acid stimulation. Interestingly, all three groups found Flcn localized to the lysosome and bound to inactive Rag GTPases only under conditions of amino acid starvation, when mTORC1 does not localize to the lysosome (Figure 3). The conclusion made from this data was that the Flcn/Fnip complex is necessary for GTP/GDP exchange in order to activate the Rag GTPases and to permit mTOR recruitment to the lysosome for activation. However, our data shows that loss of Fnip1 in kidney tissue results in hyperactivation of mTOR, which correlates

with increased microcyst formation. Furthermore, loss of Fnip1 synergizes with loss of TSC1 to hyperactive mTOR and greatly accelerates the development of PKD. Whereas tissue specific disruption of TSC1 alone in mice results in fatal PKD by 5-6 months of age, loss of both *Fnip1* and *TSC1* results in fatal PKD by 1 month of age. These results suggest that loss of Fnip1/Flcn may result in increased recruitment of mTOR to the lysosome, where it can be activated by active Rheb. In this model, disruption of TSC1, which results in constitutive activation of Rheb, would be expected to synergize with disruption of Fnip1, which increases mTOR recruitment to the lysosome for activation by Rheb. Consistent with this model, we find that *Fnip1*$^{-/-}$ heart tissue, skeletal muscle tissue, and B cells also exhibit hyperactivation of mTOR, as does loss of Flcn in renal tissue from mice and humans with BHDS. Another laboratory has also shown that AMPK via interaction with Axin and LKB1 results in tethering of AMPK/Fnip1/Flcn to the lysosomal surface in response to low glucose, where it displaces mTORC1. In this model, loss of Fnip1/Flcn could displace AMPK recruitment to the lysosome and facilitate mTORC1 recruitment and activation. Indeed, we find increased mTORC1 localization to the lysosome in Fnip1 null B cells and mouse embryonic fibroblasts (unpublished).

In summary we show for the first time that the loss of Fnip1 alone is sufficient to result in the formation of small renal cysts, defined by many of the cellular and molecular changes implicated in the development of ADPKD in humans. These changes include significant infiltration of inflammatory cells surrounding the renal cysts, decreased expression of many ion and nutrient transporters, decreased expression of cell adhesion genes, increased expression of pro-inflammatory mediators, increased activation of the mTOR and c-Myc cellular growth pathways in *Fnip1* null renal tissue. Further experimentation will be required to define the importance of these changes in the pathogenesis of PKD and renal cancer.

## Materials and Methods

### Mice

*Fnip1*$^{-/-}$, *Mb1-Cre*, *Tsc1*$^{fl/fl}$ mice were developed as previously described (Hobeika et al., 2006; Kwiatkowski et al., 2002; Park et al., 2012). Mice were housed under specific-pathogen-free conditions. All animal studies were reviewed and approved by the Institutional Animal Care and Use Committee of the University of Washington.

### Immunoblotting

Tissue for immunoblotting and RNA analyses were flash frozen and stored at -80 degrees Celsius until lysis. Frozen kidneys were homogenized in RIPA buffer (Thermo Scientific Rockford, IL) with Halt Protease and Phosphatase Inhibitor™ (Thermo Scientific Rockford, IL). Protein concentrations were determined via the Micro BCA™ Protein Assay Kit (Thermo Scientific, Rockford, IL). An equal amount of protein lysate from each sample (30-60ug) was loaded in each lane and protein components were separated via sodium dodecyl sulfate-polyacrylamide gel electrophoresis (SDS-page) through 4-12% gels Protein bands were transferred to a Immun-Blot PVFD Membrane (Bio-Rad Laboratories Hercules, CA). After blocking in 3% milk, blots were incubated overnight in primary antibodies against phospho-S6R, phospho-AMPK ser172, total AMPK, , phospho-4EBPI, (Cell Signaling Technology. Danvers, MA), followed by incubation with horseradish peroxidase-conjugated (HRP) secondary antibody. Antibody–bound proteins were visualized through SuperSignal West Pico HRP

Chemiluminescent Substrate (Thermo Scientific. Waltham, MA) activated exposure on GeneMate Blue Basic Autorad Double Emulsion Radiograph Film (Bioexpress Kaysville, UT).

**Immunohistochemistry**

Kidneys were collected and fixed in 10% formalin. All special staining was performed at the University of Washington's Histology and Imaging Core (HIC). Phospho-S6R (Cell Signaling Technology, Danvers, MA), and F4/80 (Thermo Scientific, Waltham, MA) antibodies were used.

**Quantitative PCR**

RNA was purified from frozen kidney tissue with the use of RNeasy Mini Kit (Qiagen Valenica, CA). Synthesized cDNA was yielded from RNA lysate via Invitrogen SuperScript II Reverse Transcriptase (Life Technologies Grand Island, NY). All oligonucleotide primers for RT-PCR were produced by Integrated DNA Technologies (Coralville, IA). Full primer sequences are listed in Supplemental Materials. PCR reactions were performed using the SYBR green system with annealing temperatures at 57-60$^{o}$C. Quantitative values of each sample were calculated by paired comparison of $\Delta\Delta C_T$ values (n=3-6/group).

**Seahorse assays**

Renal tubular epithelial cells (TECs) were isolated from kidneys that were collected from *Fnip1*$^{-/-}$ and *Fnip1*$^{+/-}$ (wildtype) mice that were age matched. Kidneys were dissected visually, and placed in 4 mls ice-cold Dulbecco's phosphate buffered saline (DPBS) (Gibco Grand Island, NY) and minced into pieces of ~ 1 mm$^3$. Fragments were then transferred to collagenase solution (1 mg/ml in DPBS; Sigma-Aldrich St. Louis, MO) and digested for 60 minutes at 37 $^{o}$C.

Afterwards the supernatant was sieved through a 100 μm nylon mesh. Samples were centrifuged for 5 minutes at 1250 rpm. The pellet was resuspended in ACK red cell lysis buffer (Gibco Grand Island, NY) and incubated for 2 minutes at room temperature after which 10 mls of DPBS was added, followed by centrifugation for 5 minutes at 1250 rpm. The pellet was washed twice with DPBS before plating in 10 cm dishes to a confluence of 80-90%. Cells were cultured in RPMI media (Gibco, Grand Island, NY), 10% FBS, 100 units/ ml penicillin G, 100 μg/ ml streptomycin, and 20 ng/ ml epidermal growth factor (Sigma-Aldrich St, Louis, MO). Cells were seeded on an XF96 microplate (Seahorse Biosciences) and incubated at 37 degrees Celsius for 6-12 hours prior to analysis. Mitochondrial function was analyzed in accordance with the XF Cell Mito Stress Test Kit (Seahorse Biosciences) and basal respiratory and glycolytic rates were determined. Following basal measurements, multiple assays reagents were added including: carbonyl cyanide 4-(trifluoromethoxy) phenylhydrazone (FCCP; Sigma C2920) and Antimycin.

**Metabolomics**

Mass spectrometry experiments were performed in the Northwest Metabolomics Research Center at the University of Washington. 5-8 mg samples of frozen gastrocnemius muscle collected from age and matched *Fnip1*$^{-/-}$ and *Fnip1*$^{+/-}$ (wildtype) control mice were homogenized in 50% methanol at $^{-}80^{o}$C (n=4/group). Results were normalized based on tissue weight. Acetonitrile, ammonium acetate, and acetic acid (LC-MS grade) were all purchased from Fisher Scientific (Pittsburgh, PA). The standard compounds corresponding to the measured metabolites were purchased from Sigma-Aldrich (Saint Louis, MO) and Fisher Scientific (Pittsburgh, PA). Stable isotope-labeled tyrosine and lactate internal standards (L-tyrosine-$^{13}C_2$ and sodium-L-lactate-$^{13}C_3$) were purchased from Cambridge Isotope Laboratories, Inc. (Tewksbury, MA). The

purities of non-labeled standards were >95-99% whereas the purities of the two $^{13}C$ labeled compounds were > 99%.

The LC system was composed of two Agilent 1260 binary pumps, an Agilent 1260 auto-sampler, and Agilent 1290 column compartment containing a column-switching valve (Agilent Technologies, Santa Clara, CA). Each sample was injected twice, 10 µL for analysis using negative ionization mode and 2 µL for analysis using positive ionization mode. Both chromatographic separations were performed in hydrophilic interaction chromatography (HILIC) mode on two SeQuant ZIC-cHILIC columns (150 x 2.1 mm, 3.0 µm particle size, Merck KGaA, Darmstadt, Germany) connected in parallel. Our setup allows one column performing separation while the other column is getting reconditioned and ready for the next injection. The flow rate was 0.300 mL/min, auto-sampler temperature was kept at 4 $^{o}$C, the column compartment was set at 40℃, and total separation time for both ionization modes was 20 min. The mobile phase was composed of Solvents A (5 mM ammonium acetate in 90%$H_2O$/ 10% acetonitrile + 0.2% acetic acid) and B (5 mM ammonium acetate in 90%acetonitrile/ 10% $H_2O$ + 0.2% acetic acid). The gradient conditions for both separations were identical and are shown as follows:

| Time Segment, min. | Solvent A, % | Solvent B, % |
|---|---|---|
| 0 - 2 | 25 | 75 |
| 2 - 5 | from 25 to 70 | from 75 to 30 |
| 5 - 9 | 70 | 30 |
| 9 - 11 | from 70 to 25 | from 30 to 75 |
| 11 - 20 | 25 | 75 |

The metabolite identities were confirmed by spiking the pooled serum sample used for method development with mixtures of standard compounds (each mixture contained five standard metabolites). However, some metabolites that could not be well separated and had similar m/z values (<1 Da) were integrated as single peaks (e.g., malonic acid and 3-hydroxybutyric acid were reported as a single peak).

After the chromatographic separation, MS ionization and data acquisition were performed using an AB Sciex QTrap 5500 mass spectrometer (AB Sciex, Toronto, ON, Canada) equipped with an electrospray ionization (ESI) source. The instrument was controlled by Analyst 1.5 software (AB Sciex, Toronto, ON, Canada). Targeted data acquisition was performed in multiple-reaction-monitoring (MRM) mode. We monitored 99 and 59 MRM transitions in negative and positive mode, respectively (158 transitions in total). The source and collision gas was $N_2$ (99.999% purity). The ion source conditions in negative/positive mode were: curtain gas (CUR) = 25 psi, collision gas (CAD) = high, ion spray voltage (IS) = - 3.8/3.8 KV, temperature (TEM) = 500 $^{o}$C, ion source gas 1 (GS1) = 50 psi, and ion source gas 2 (GS2) = 40 psi. The extracted MRM peaks were integrated using MultiQuant 2.1 software (AB Sciex, Toronto, ON, Canada).

**RNAseq**

RNA was purified from frozen kidney tissue with the use of RNeasy Mini Kit (Qiagen Valenica, CA). Total RNA integrity was checked using an Agilent 2200 TapeStation (Agilent Technologies, Inc., Santa Clara, CA) and quantified using a Trinean DropSense96 spectrophotometer (Caliper Life Sciences, Hopkinton, MA).

RNA-seq libraries were prepared from total RNA using the TruSeq RNA Sample Prep Kit (Illumina, Inc., San Diego, CA, USA) and a Sciclone NGSx Workstation (PerkinElmer,

Waltham, MA, USA). Library size distributions were validated using an Agilent 2200 TapeStation (Agilent Technologies, Santa Clara, CA, USA). Additional library QC, blending of pooled indexed libraries, and cluster optimization were performed using Life Technologies' Invitrogen Qubit® 2.0 Fluorometer (Life Technologies-Invitrogen, Carlsbad, CA, USA). RNA-seq libraries were pooled (6-plex) and clustered onto a flow cell lane. Sequencing was performed using an Illumina HiSeq 2500 in rapid mode employing a paired-end, 50 base read length (PE50) sequencing strategy.

**Transmission electron microscopy**

Kidneys were harvested from 8 week-old *Fnip1*$^{-/-}$ and *Fnip1*$^{+/-}$ (wildtype) mice were chopped into ~ 1 mm$^3$ pieces and preserved in Karnovsky's Gluteraldehyde fixative. Samples were dehydrated, sectioned into 70-100nm sections at the Vision Core Lab of the University of Washington (Seattle, WA). Tissue slices were epoxy embedded and visualized with the use of a JEOL 1230 transmission electron microscope (JEOL Ltd., Tokyo, JAPAN).

**Figures**

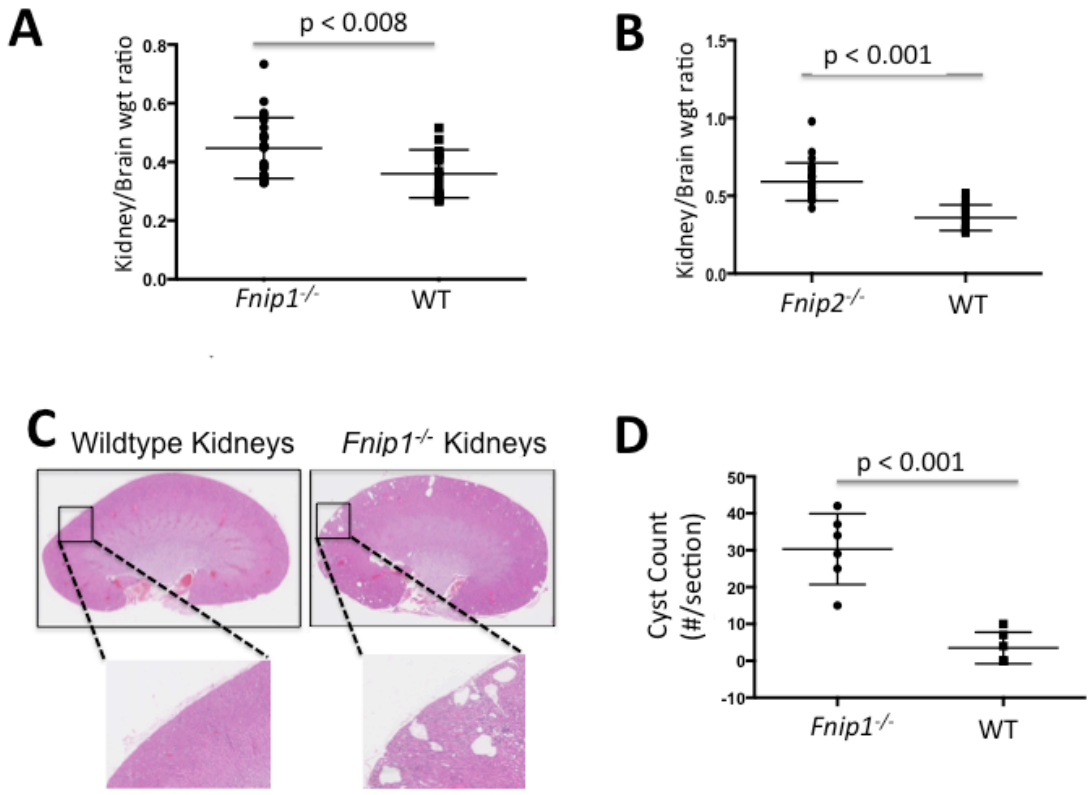


**Figure 1. Loss of Fnip1 results in formation of microcysts, and increased kidney size.** Kidney-to-Brain weight ratios of :(A) *Fnip1*$^{-/-}$ vs wildtype , and (B) *Fnip2*$^{-/-}$ vs wildtype, showing that loss of either Fnip1 or Fnip2 results in increased kidney size. (C) Representative images of histology sections of *Fnip1*$^{-/-}$ and wildtype kidneys showing cyst formation in the renal cortex of the *Fnip1*$^{-/-}$ kidneys. (D) Graph showing cyst counts by a blinded counter of *Fnip1*$^{-/-}$ (n=3) and wildtype (n=3) kidneys. *P-values are shown.

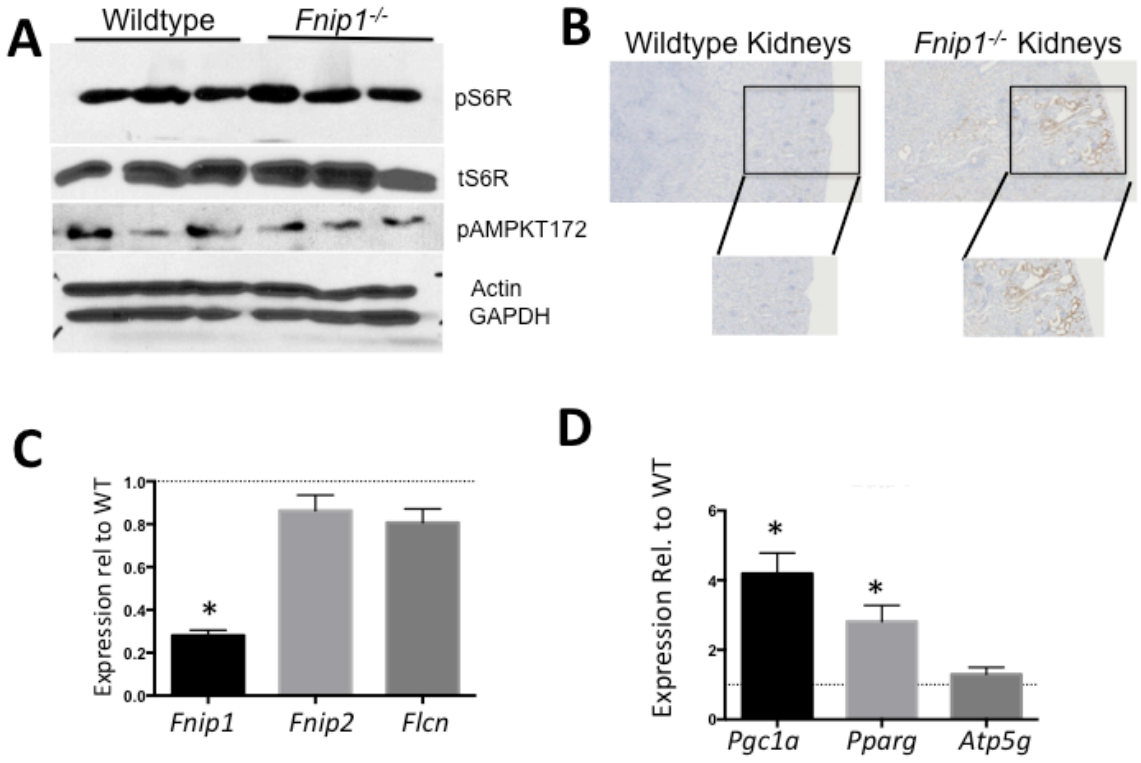


**Figure 2. Increased mTOR activation in Fnip1 null kidney tubular epithelial cells (TECs).** (A) Immunoblots showing normal mTOR and AMPK activation in total renal tissue. (B) Representative immunohistochemistry images showing increased p-S6R activation around cystic tubules in *Fnip1*$^{-/-}$ mice, (C) Realtime PCR showing no significant changes in *Flcn* and *Fnip2* though a significant decrease in *Fnip1* mRNA expression in *Fnip1*$^{-/-}$ renal tissue, and (D) realtime PCR showing significant increases in *Pgc1α* and *Pparg* (n= 3, *= p<0.01).

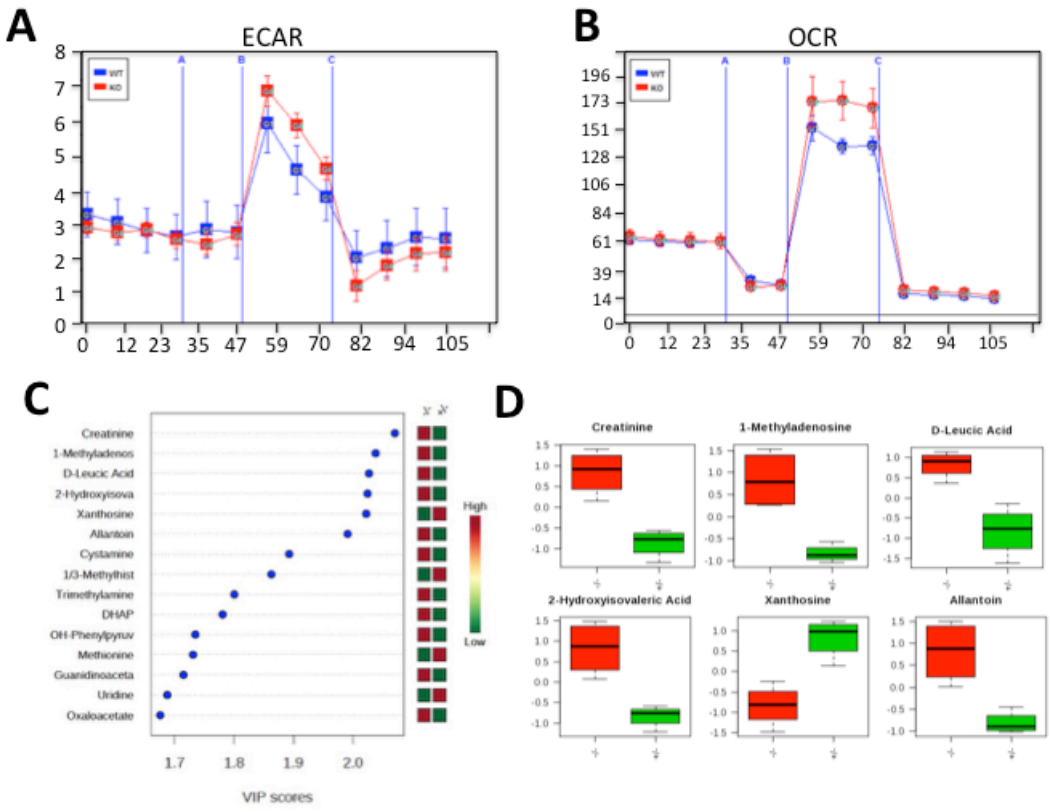


**Figure 3**. ***Fnip1*$^{-/-}$ kidney tubular epithelial cells exhibit increased metabolism.**
(A)Seahorse analyses showing increased glycolysis (B) and oxidative phosphorylation within cultured *Fnip1*$^{-/-}$ TECs. (C and D) VIP scores of metabolite changes in *Fnip1*$^{-/-}$ versus wildtype renal tissue showing changes in nitrogenous waste products, amino acid metabolites, glycolysis, and TCA cycle metabolites (n=3 each genotype).

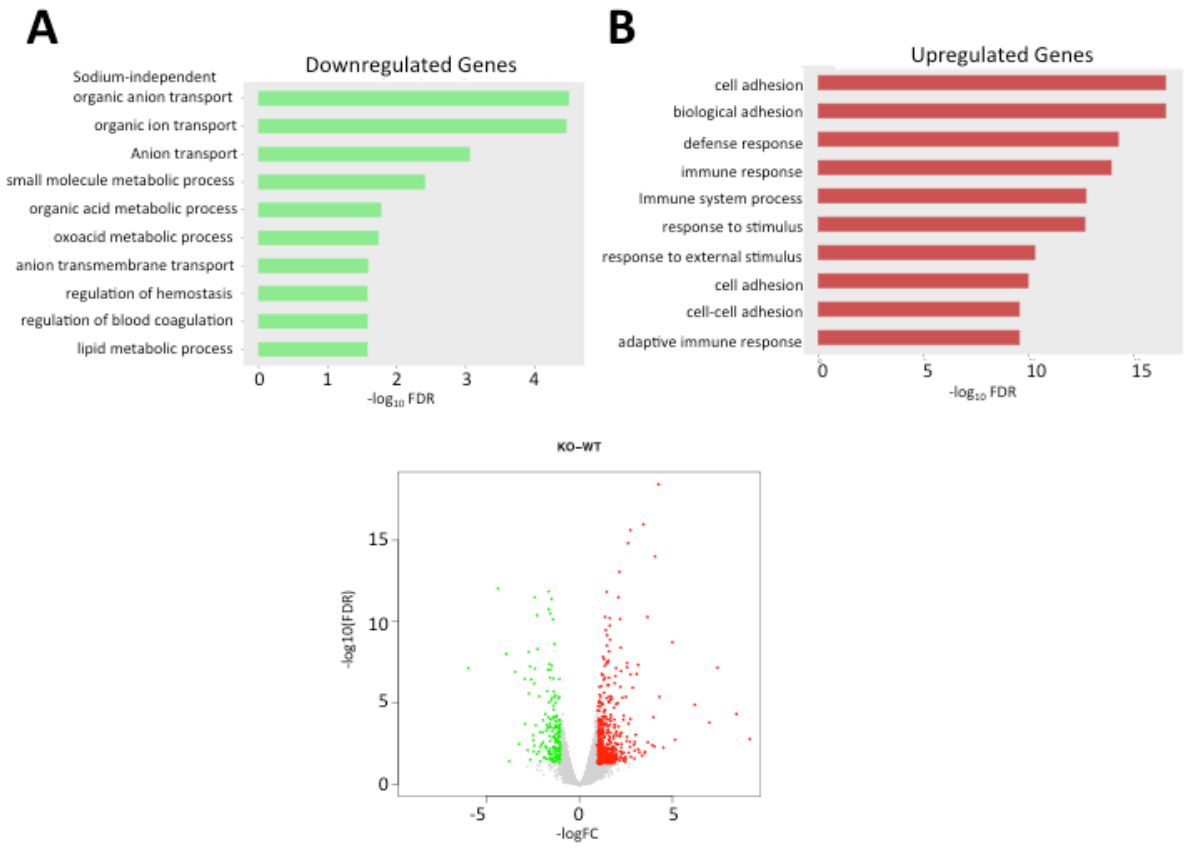


**Figure 4. RNAseq of *Fnip1*$^{-/-}$ versus wildtype renal tissue.**
RNAseq was performed on kidney tissue from *Fnip1*$^{-/-}$ and wildtype mice. KEGG analysis showing: (A) significantly decreased expression of genes grouped by expression levels and gene function, and (B) significantly increased expression of genes grouped by expression levels and gene function. (n=3 of each genotype). The most significantly decreased genes were involved in ion transport and metabolism, whereas the most significantly increased genes were involved in cell adhesion and immune responses.

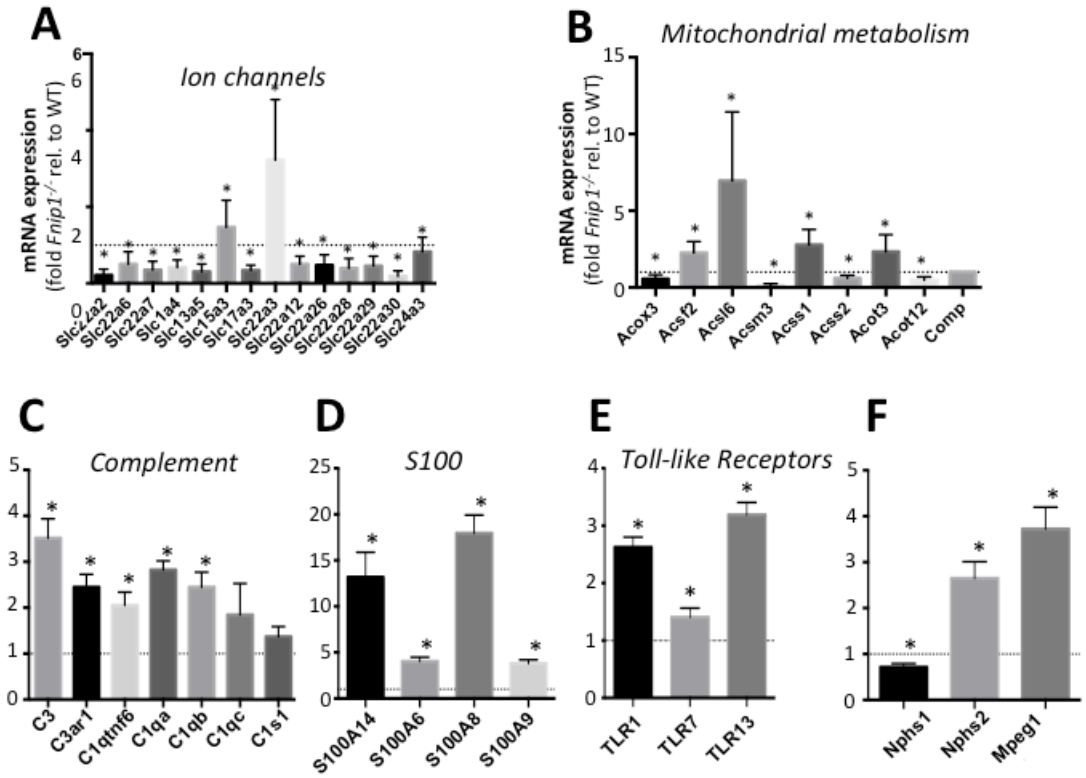


**Figure 5. Realtime PCR analyses on kidney tissue from *Fnip1*$^{-/-}$ versus wildtype mice**
(A) Decreased expression of genes encoding many of the solute carrier family of transporter proteins, (B) altered expression of genes coding acyl-CoA genes that are responsible for metabolism of fatty acids, (C) increased expression of complement 3 and 1 genes, (D) Increased expression of S100A genes including A14, 6, 8, and 9, (E) Increased expression of TLR1,7, and 13 genes, and (F) altered expression of genes encoding essential renal function genes. (n=3 of each genotype, *= $p<0.01$)

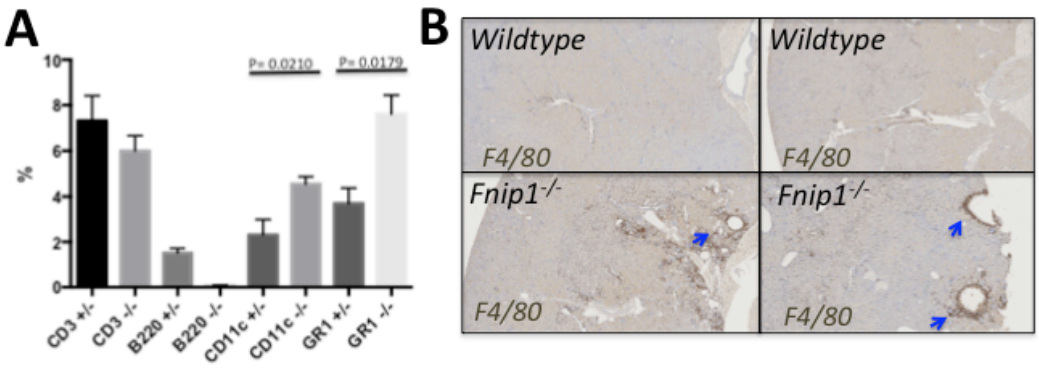


**Figure 6. Increased immune cell infiltration in *Fnip1*$^{-/-}$ null kidney tissue.**
(A) Flow cytometric analyses of immune cells isolated from *Fnip1*$^{-/-}$ and wildtype kidney tissue showing increases in CD11c and GR1 labeled cells though decreases in CD3 and B220 labeled cells (n=3 of each genotype, p-values are shown). (B) Representative immunohistochemistry images showing increased myeloid cells localized around renal cysts of *Fnip1*$^{-/-}$ mice (arrows).

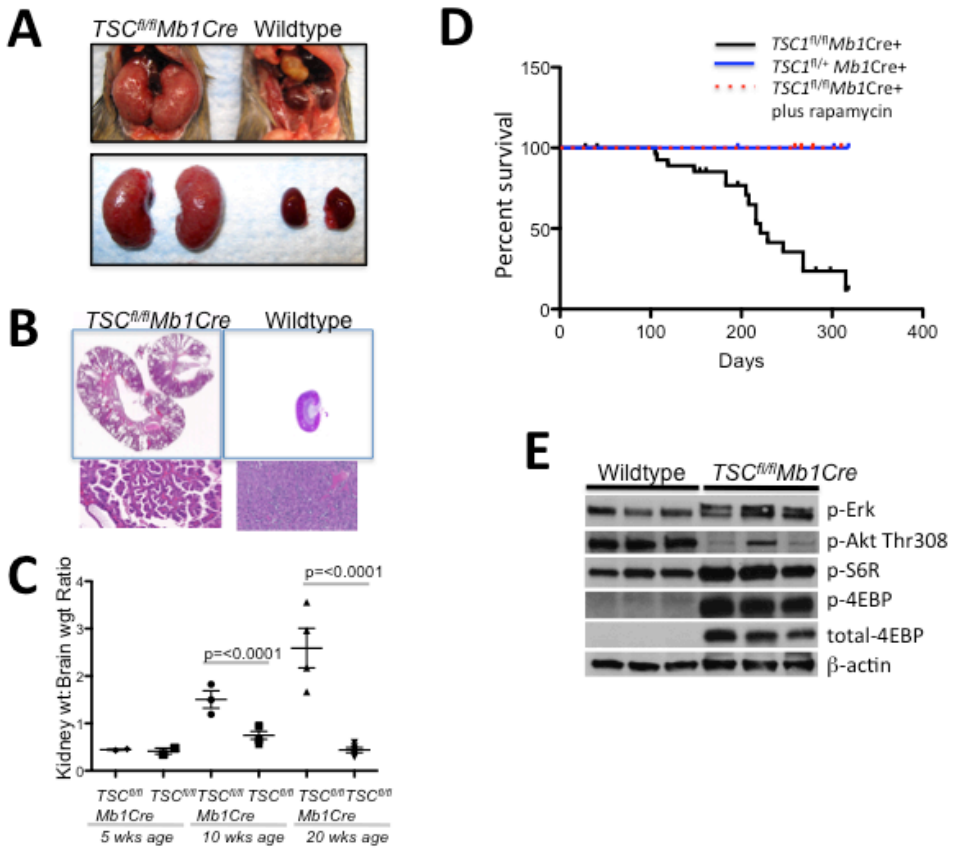


**Figure 7. Conditional disruption of *Tsc1* results in polycystic kidney disease.**

(A) Representative gross pictures of *Tsc1*$^{fl/fl}$ *Mb1Cre*+ and WT kidneys showing that loss of *Tsc1* results in kidney enlargement in 20-week old mice. (B) Representative histology images of *Tsc1*$^{fl/fl}$ *Mb1Cre*+ kidneys showing development of polycystic kidney disease by 20 weeks of age. (C) Kidney-to-brain ratio graph showing ratios at 5, 10, and 20 week old *Tsc1*$^{fl/fl}$ *Mb1Cre*+ and WT mice showing a gradual increase in kidney-to-brain weight ratio in *Tsc1*$^{fl/fl}$ *Mb1Cre*+ kidneys. (D) Survival graph of *Tsc1*$^{fl/fl}$ *Mb1Cre*+ (solid black line), *Tsc1*$^{fl/+}$ *Mb1Cre*+ (sold blue line), and rapamycin treated *Tsc1*$^{fl/fl}$ *Mb1Cre*+ (dotted red line) showing that polycystic kidney disease is fatal though the phenotype is rescued by rapamycin. (E) Immunoblots of proteins isolated from whole kidney lysates showing increased activation of P-S6R and p-4EBP that are activated by mTORC1 indicated activation of the pathway in *Tsc1*$^{fl/fl}$ *Mb1Cre*$^{+}$ kidney tissue. (n=3 each genotype, p-values are shown)

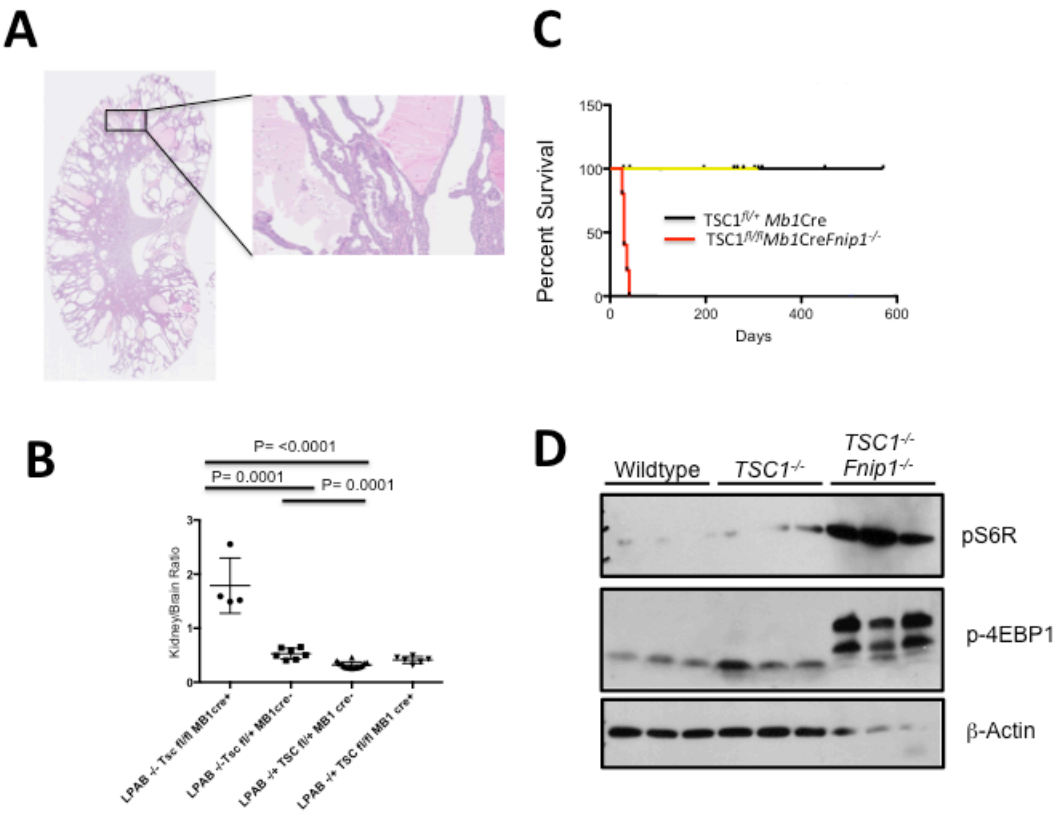


**Figure 8**. **Loss of Fnip1 synergizes with loss of TSC1 resulting in accelerated PKD and mTOR activation.**
(A) Representative histology image of *Tsc1*$^{fl/fl}$ *Mb1Cre*$^{+}$*Fnip1*$^{-/-}$ double null mice that shows the development of severe polycystic kidney disease at 5 weeks of age. (B) Kidney-to-brain ratio graph comparing; double null (LPAB$^{-/-}$ *Tsc1*$^{fl/fl}$ *Mb1Cre*$^{+}$*Fnip1*$^{-/-}$), *Fnip1*$^{-/-}$ (LPAB$^{-/-}$ *Tsc1*$^{fl/+}$ *Mb1Cre*-), Tsc1 null (LPAB$^{-/+}$ *Tsc1*$^{fl/fl}$ *Mb1Cre*$^{+}$), and wildtype (LPAB$^{-/+}$ *Tsc1*$^{fl/+}$ *Mb1Cre*$^{-}$) at 5 weeks of age, showing a large increase in kidney size of the double null mice at a early age, (C) survival graph of double null, and wildtype mice showing early death in double null mice due to severe polycystic kidney disease. (D) Immunoblots of proteins isolated from whole kidney lysates wildtype, *TSC1*$^{-/-}$, and *TSC1*$^{-/-}$ *Fnip1*$^{-/-}$ blots show an increase of pS6R and p-4EBP over that of the *TSC1*$^{-/-}$ indicating a hyperactivation of the mTOR pathway. (n=3 each genotype, p-values are shown)

**References**


Anders, H.J., and Ryu, M. (2011). Renal microenvironments and macrophage phenotypes determine progression or resolution of renal inflammation and fibrosis. Kidney Int *80*, 915-925.

Appleby, M.W., and Ramsdell, F. (2003). A forward-genetic approach for analysis of the immune system. Nat Rev Immunol *3*, 463-471.

Chapin, H.C., and Caplan, M.J. (2010). The cell biology of polycystic kidney disease. J Cell Biol *191*, 701-710.

Chen, J., Futami, K., Petillo, D., Peng, J., Wang, P., Knol, J., Li, Y., Khoo, S.K., Huang, D., Qian, C.N.*, et al.* (2008). Deficiency of FLCN in mouse kidney led to development of polycystic kidneys and renal neoplasia. PloS one *3*, e3581.

Chen, J., Huang, D., Rubera, I., Futami, K., Wang, P., Zickert, P., Khoo, S.K., Dykema, K., Zhao, P., Petillo, D.*, et al.* (2015). Disruption of tubular Flcn expression as a mouse model for renal tumor induction. Kidney Int *88*, 1057-1069.

Goncharova, E.A., Goncharov, D.A., James, M.L., Atochina-Vasserman, E.N., Stepanova, V., Hong, S.B., Li, H., Gonzales, L., Baba, M., Linehan, W.M.*, et al.* (2014). Folliculin controls lung alveolar enlargement and epithelial cell survival through E-cadherin, LKB1, and AMPK. Cell reports *7*, 412-423.

Han, S.H., Malaga-Dieguez, L., Chinga, F., Kang, H.M., Tao, J., Reidy, K., and Susztak, K. (2016). Deletion of Lkb1 in Renal Tubular Epithelial Cells Leads to CKD by Altering Metabolism. J Am Soc Nephrol *27*, 439-453.

Harris, P.C., and Torres, V.E. (2014). Genetic mechanisms and signaling pathways in autosomal dominant polycystic kidney disease. J Clin Invest *124*, 2315-2324.

Hartman, T.R., Liu, D., Zilfou, J.T., Robb, V., Morrison, T., Watnick, T., and Henske, E.P. (2009). The tuberous sclerosis proteins regulate formation of the primary cilium via a rapamycin-insensitive and polycystin 1-independent pathway. Human molecular genetics *18*, 151-163.

Hasumi, H., Baba, M., Hasumi, Y., Huang, Y., Oh, H., Hughes, R.M., Klein, M.E., Takikita, S., Nagashima, K., Schmidt, L.S.*, et al.* (2012). Regulation of mitochondrial oxidative metabolism by tumor suppressor FLCN. Journal of the National Cancer Institute *104*, 1750-1764.

Hasumi, H., Baba, M., Hasumi, Y., Lang, M., Huang, Y., Oh, H.F., Matsuo, M., Merino, M.J., Yao, M., Ito, Y.*, et al.* (2015). Folliculin-interacting proteins Fnip1 and Fnip2 play critical roles in

kidney tumor suppression in cooperation with Flcn. Proceedings of the National Academy of Sciences of the United States of America *112*, E1624-1631.

Hasumi, H., Baba, M., Hong, S.B., Hasumi, Y., Huang, Y., Yao, M., Valera, V.A., Linehan, W.M., and Schmidt, L.S. (2008). Identification and characterization of a novel folliculin-interacting protein FNIP2. Gene *415*, 60-67.

Hasumi, Y., Baba, M., Ajima, R., Hasumi, H., Valera, V.A., Klein, M.E., Haines, D.C., Merino, M.J., Hong, S.B., Yamaguchi, T.P.*, et al.* (2009). Homozygous loss of BHD causes early embryonic lethality and kidney tumor development with activation of mTORC1 and mTORC2. Proceedings of the National Academy of Sciences of the United States of America *106*, 18722-18727.

Hobeika, E., Thiemann, S., Storch, B., Jumaa, H., Nielsen, P.J., Pelanda, R., and Reth, M. (2006). Testing gene function early in the B cell lineage in mb1-cre mice. Proceedings of the National Academy of Sciences of the United States of America *103*, 13789-13794.

Karihaloo, A., Koraishy, F., Huen, S.C., Lee, Y., Merrick, D., Caplan, M.J., Somlo, S., and Cantley, L.G. (2011). Macrophages promote cyst growth in polycystic kidney disease. J Am Soc Nephrol *22*, 1809-1814.

Kwiatkowski, D.J., Zhang, H., Bandura, J.L., Heiberger, K.M., Glogauer, M., el-Hashemite, N., and Onda, H. (2002). A mouse model of TSC1 reveals sex-dependent lethality from liver hemangiomas, and up-regulation of p70S6 kinase activity in Tsc1 null cells. Human molecular genetics *11*, 525-534.

Mostov, K.E. (2006). mTOR is out of control in polycystic kidney disease. Proceedings of the National Academy of Sciences of the United States of America *103*, 5247-5248.

Nickerson, M.L., Warren, M.B., Toro, J.R., Matrosova, V., Glenn, G., Turner, M.L., Duray, P., Merino, M., Choyke, P., Pavlovich, C.P.*, et al.* (2002). Mutations in a novel gene lead to kidney tumors, lung wall defects, and benign tumors of the hair follicle in patients with the Birt-Hogg-Dube syndrome. Cancer Cell *2*, 157-164.

Park, H., Staehling, K., Tsang, M., Appleby, M.W., Brunkow, M.E., Margineantu, D., Hockenbery, D.M., Habib, T., Liggitt, H.D., Carlson, G.*, et al.* (2012). Disruption of Fnip1 reveals a metabolic checkpoint controlling B lymphocyte development. Immunity *36*, 769-781.

Pavlovich, C.P., Walther, M.M., Eyler, R.A., Hewitt, S.M., Zbar, B., Linehan, W.M., and Merino, M.J. (2002). Renal tumors in the Birt-Hogg-Dube syndrome. Am J Surg Pathol *26*, 1542-1552.

Pema, M., Drusian, L., Chiaravalli, M., Castelli, M., Yao, Q., Ricciardi, S., Somlo, S., Qian, F., Biffo, S., and Boletta, A. (2016). mTORC1-mediated inhibition of polycystin-1 expression drives renal cyst formation in tuberous sclerosis complex. Nat Commun *7*, 10786.

Seeger-Nukpezah, T., Geynisman, D.M., Nikonova, A.S., Benzing, T., and Golemis, E.A. (2015). The hallmarks of cancer: relevance to the pathogenesis of polycystic kidney disease. Nat Rev Nephrol *11*, 515-534.

Shillingford, J.M., Murcia, N.S., Larson, C.H., Low, S.H., Hedgepeth, R., Brown, N., Flask, C.A., Novick, A.C., Goldfarb, D.A., Kramer-Zucker, A.*, et al.* (2006). The mTOR pathway is regulated by polycystin-1, and its inhibition reverses renal cystogenesis in polycystic kidney disease. Proceedings of the National Academy of Sciences of the United States of America *103*, 5466-5471.

Trudel, M., D'Agati, V., and Costantini, F. (1991). C-myc as an inducer of polycystic kidney disease in transgenic mice. Kidney Int *39*, 665-671.

Zhou, J., Brugarolas, J., and Parada, L.F. (2009). Loss of Tsc1, but not Pten, in renal tubular cells causes polycystic kidney disease by activating mTORC1. Human molecular genetics *18*, 4428-4441.